Advanced Robotics, Vol. 20, No. 8, pp. 933–951 (2006)

Also available online - www.vsppub.com

Short paper

Robot-assisted evaluation of coordination between grasp and load forces in a power grasp in humans

JANEZ PODOBNIK * and MARKO MUNIH

Laboratory of Robotics and Biomedical Engineering, Faculty of Electrical Engineering, University of Ljubljana, Trzaska c. 25, 1001 Ljubljana, Slovenia

Received 4 July 2005; accepted 7 October 2005

Abstract—A novel approach for evaluation of a grasp in humans is presented. The key novelty is combination of a haptic interface with force/torque transducers for measuring the grasp force. This paper presents results of grasp and load force coordination for quasi-static and dynamic external load force disturbances for a power grasp. An elevation of the grasp force is observed in a dynamic task. Elevation of the grasp force is needed for an additional safety margin to ensure a stable grasp.

Keywords: Grasp force; power grasp; haptic interface; tracking; stable grasp.

1. INTRODUCTION

The similarity of a multi-fingered robot hand with a human hand and the superior ability of human grasping [1] with respect to robotic grasping has been often employed in research on a grasp strategy of a robot hand on the basis of human motion and grasping [2–7].

For successful execution of the task, a certain degree of quality of the grasp has to be maintained [8] and four essential properties (dexterity, equilibrium, stability and dynamic behavior) of the grasp must be controlled [9]. A grasp is stable when:

- Forces and moments are exerted on the object in a way to move it or to keep it in a stable equilibrium [10].
- It is able to resist self and externally generated load forces that act on the grasped object [4, 9].
- An object returns to its equilibrium position after load force disturbances [4, 9].

The grasp that meets this conditions is a force-closure grasp [10]. Nguyen [10] also showed that non-marginal equilibrium grasps are force-closure grasps.

*To whom correspondence should be addressed. E-mail: janez.podobnik@robo.fe.uni-lj.si

The problem of real-time force-closure grasp planning on arbitrary objects is recognized as an essential component of dexterous manipulation and grasping with multi-fingered robot hands [11]. Hence, the question of human grasping behavior and the strategy for maintaining a stable grasp in humans is of interest in robot grasping research [4].

The grasp force is limited to the normal force component exerted on the surface of the held object, while the load force is the tangential force tending to cause slippage [12]. A series of experiments performed in order to study coordination between the grasp force and load force showed that humans use a safety margin against frictional slips. It has been also shown that the safety margin is small to avoid excessive grasp forces [13–16].

Napier [1] defined two major grasp prehensile postures: precision grasp and power grasp. The two grasps differ in evolutional, anatomical, functional and task features. The power grasp meets power requirements to apply forces and resist arbitrary forces on the grasped object to assure stability, while the precision grasp meets precision requirements which involve fine adjustments of posture and the emphasis is on the dexterity. A number of researchers have investigated the precision grasp, whereas the power grasp is less often an object of research. In case of the precision grasp the experimental setup requires minimization of the measuring system, whereas in the case of the power grasp the experimental setup must provide actuators for producing high load forces and a measuring system to measure high grasp forces.

The novel technique presented here enables the investigation of grasping for wide range of grasp forces. This paper introduces a new robot-assisted technique for evaluation of a grasp in humans. The main contribution is the use of a haptic interface with a particular setup of force/torque transducers for measuring grasp forces. The unique characteristics of haptic interfaces to render kinesthetic information to the human operator interacting with virtual environments [17] allows programming and generating external load forces, and defining exact dynamics of a virtual environment. Use of an admittance haptic display allows generation of high external load forces; relatively heavy force/torque transducers for measuring wide range of grasp forces can be mounted on a robot tool end. A transparent admittance control algorithm is used to compensate for the dynamics of the attached measuring equipment, while maintaining the predefined dynamics of the virtual environment.

This paper presents new results filling the missing gap in the area of coordination between the grasp force and high external load force under quasi-static and dynamic conditions. During the quasi-static and dynamic load force conditions the subject employs a strategy of grasp and load force coordination that is adjusted to the dynamics of the load force. As a consequence, this results in distinctive shapes of plots of grasp *versus* load force representation: a line in the case of quasi-static load force and a triangle in the case of dynamic load force.

2. METHODS

2.1. Admittance haptic interface

A general purpose haptic interface based on a modified industrial robot (Stäubli RX90) was used in this study. The haptic interface was developed in the Laboratory of Robotics and Biomedical Engineering in order to display a wide range of impedances for the arm-size haptic interactions. Arm movements in a haptic environment require a powerful and high Z-width force generator with a workspace similar to that of the human arm [18]. The workspace of the Stäubli RX90 covers a larger part of the human operators arm workspace. The architecture incorporating a PC controller allows the design of custom-made algorithms implemented on RTlinux with 4-kHz sampling loop frequency. A 6-d.o.f. digital JR3 85M35A-I40 force/torque sensor for measuring the contact force is attached between the handle and the tip of the manipulator. JR3 sensors are extremely stiff, resulting in minimal degradation of system dynamics and positioning accuracy [19]. This allows the high transparency needed to present quality haptic interaction.

2.2. Model of the virtual environment

A general purpose 6-d.o.f. haptic interface allows use of an arbitrary virtual environment, where force is an input and velocity is an output. The virtual environment can be described with a mechanical admittance (1) having mass m, damping b and stiffness k:

$$V(s) = A(s)F(s) = \frac{F(s)}{ms + b + \dfrac{k}{s}}. \tag{1}$$

Equation (1) shows that the mechanical admittance can be represented as a second-order filter with one zero. Adding another zero to the admittance filter gives a second-order causal filter with two zeros. If force is filtered with a filter with added zero, the acceleration can be computed. This is an advantage of admittance-type haptic interfaces in comparison with impedance-type haptic interfaces where velocity must be calculated by differentiating the position and acceleration by differentiating the velocity.

The experiments were performed in a virtual environment consisting of a mass $m = 1$ kg on the long beam with finite stiffness $k = 15\,000$ N/m in the transversal direction and surface with friction $b = 50$ Ns/m. Figure 1 shows a graphical representation and (2) gives a mathematical description of the virtual environment:

$$A(s) = \begin{cases} \dfrac{1}{ms + b}, & x\text{-direction (along beam)} \\ \dfrac{1}{ms + b + \dfrac{k}{s}}, & y, z\text{-direction.} \end{cases} \tag{2}$$

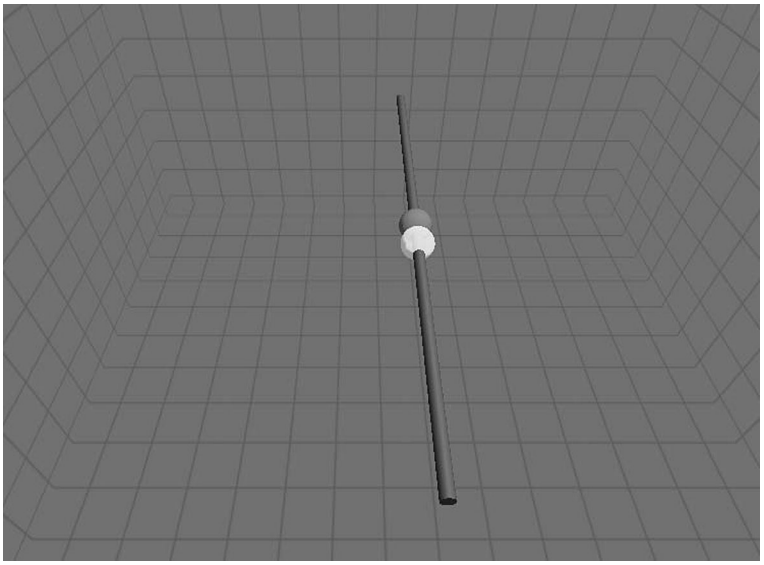

Figure 1. Virtual environment with a mass on a long beam with a frictional surface. The dark sphere is a position reference and the bright transparent sphere is an actual position.

The input force to the control algorithm of the haptic display is sum of a contact force F_{L} measured with the 6-d.o.f. digital JR3 85M35A-I40 force/torque sensor and virtual force F_{virt}. The F_{L} is the force applied by the human operator. The virtual force F_{virt} is programable and is therefore purely virtual. Hence, if virtual force is set to $F_{\mathrm{virt}} = -10$ N then the human operator must pull towards himself with a force $F_{\mathrm{L}} = 10$ N to keep the end point of manipulator in the equilibrium position.

The full dynamic model of the virtual environment accounting force F_{L} and force F_{virt} in the time domain is:

$$\begin{aligned} F_{\mathrm{L},x} + F_{\mathrm{virt},x} &= m\,a_x + b\,v_x \\ F_{\mathrm{L},y} + F_{\mathrm{virt},y} &= m\,a_y + b\,v_y + k\,p_y \\ F_{\mathrm{L},z} + F_{\mathrm{virt},z} &= m\,a_z + b\,v_z + k\,p_z, \end{aligned} \tag{3}$$

where a, v and p denote, respectively, the acceleration, velocity and position, and x, y and z denote the axes of the coordinate system of the virtual environment.

2.3. Hand grasp force measuring system

A specially designed handle for measuring grasp forces was used. Three 6-d.o.f. JR3 50M31A-I25 digital force/torque sensors were mounted on the tool end fitted on the robot. The cylindrical handle was split into three beams and each beam was attached to a separate JR3 sensor. Figure 2 shows a handle with force/torque sensors. A symmetrical arrangement of three beams (oriented at 120° around the

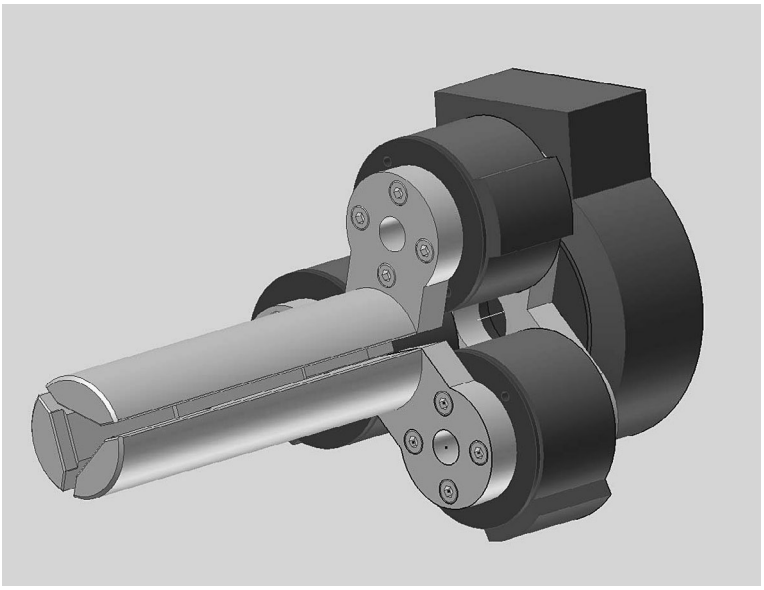

Figure 2. Hand grasp force measuring system.

center) allows the quantification of the grasp force independently from the hand grasp position and orientation. A minimum set of three beams is needed to achieve this [20].

The setup has a low noise level, each sensor measures forces/torques in range of $[-150, 150]$ N/$[-8, 8]$ Nm. Measured grasp forces are assumed to be radial [21]. Hence, grasp force F_G is the sum of forces acting on each beam in the radial direction.

A smooth layer of tape was attached to the each aluminium beam surface to assure uniform friction conditions for each beam. The size of the handle diameter was 35 mm, which was found to be the optimal size handle diameter for achieving maximum strength [22].

2.4. Subjects

Five healthy male, right-handed subjects (23–29 years old) participated in the present study. The participants had no history of neuromuscular or musculoskeletal disorders related to the upper extremities and gave their informed consent to participate.

2.5. Procedures

Subjects, that were seated comfortably in a chair in front of and outside of the robot workspace, were instructed to grasp the handle. The end-point position of the robot was adjusted to make a comfortable grasp with the shoulder at 45° flexion

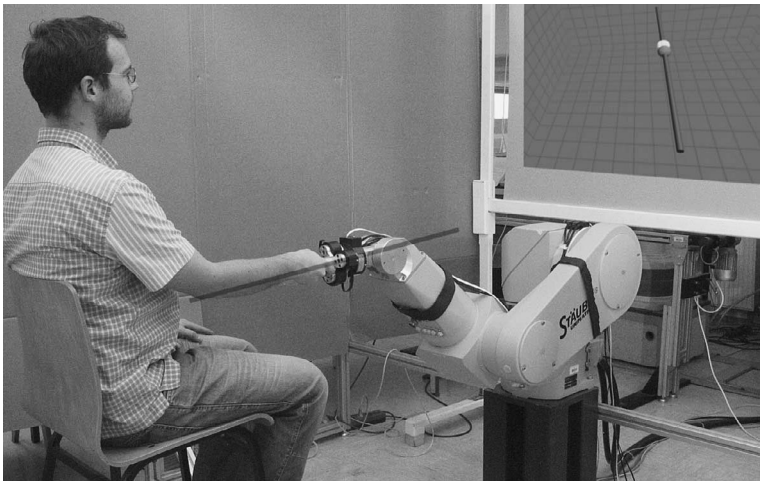

Figure 3. Experimental conditions. In the center of the picture is the hand grasp measuring system. The subject is grasping the hand grasp force measuring handle and observing the position of the end-point of the robot relative to the reference position. The dark line shows the direction of movements.

and the elbow at 135° flexion, with the forearm and wrist in a neutral position (see Fig. 3). Participants washed their hands with liquid soap and dried them prior to the experimental sessions. Subject gave a sign for the start of the experiments, when the grasp was comfortable and stable.

Each subject was instructed to keep the position in the starting reference position. Information about the position of the end-point was graphically projected on the screen in front of the subject (see Fig. 3). After each trial, a short rest was taken and after four trials a longer rest was taken to eliminate the effects of fatigue. After each trial the subject was instructed to wipe his hands with a paper towel.

Two courses of virtual force *versus* time were used: ramp (quasi-static) and sinusoidal (dynamic experiment). In the ramp experiment the virtual force F_{virt} was linearly increasing from 0 to 100 N in 25 s. In the sinusoidal experiment the virtual force was ramp multiplied with a sinus having a frequency of 0.5 Hz with amplitude increasing from 0 to 50 N and mean value increasing from 0 to 50 N in 25 s (see Fig. 4). Ramp task is used to study the ability to follow-up a smooth gradual increase of the grasp force and sinus shape to study the ability to coordinate the grasp force with the load force in a dynamic load force environment [23]. Each of the two experiments was repeated 4 times and trials were performed in random order. The subject was not informed which type of experiment would be performed next to minimize any learning effect. Later the experiments were repeated, but with decreasing the amplitude from 100 to 0 N for the ramp and sinusoidal experiments. This enabled us to examine the grasp and load coordination also when amplitude is decreasing.

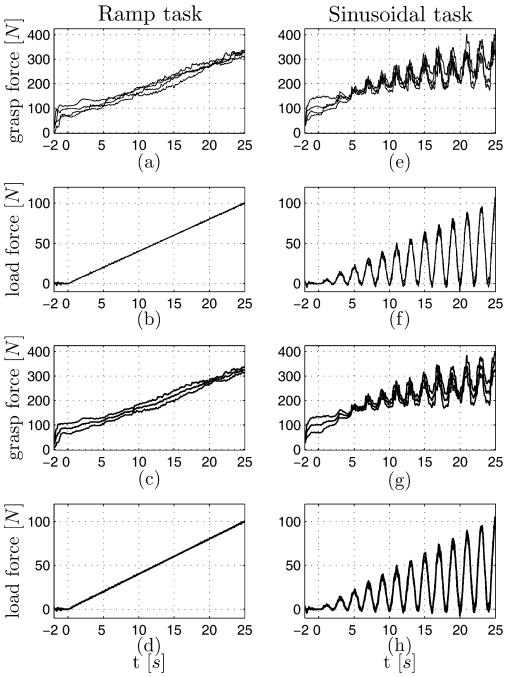

Figure 4. Results for subject 1. Four experimental trials for the ramp task: (a) grasp forces, (b) load forces. Four experimental trials for the sinusoidal task: (e) grasp forces, (f) load forces. Mean and standard deviations for the four trials: (c) grasp force — ramp task, (d) load force — ramp task; (g) grasp force — sinusoidal task, (h) load force — sinusoidal task.

3. RESULTS

Several different measures were used to asses the performance of the position-tracking task. Figure 4 shows results for subject 1. Figure 4a, b, e and f shows courses for four experimental trials for the ramp and sinusoidal tasks (grasp and load forces) when the amplitude is increasing. Figure 4c, d, g and h display the mean (dark line) and standard deviations (light grey lines) for upper trials.

It is important to note that grasp force F_{G} is the sum of the forces acting radially on the beams of the hand grasp force measuring system, while the load force F_{L} is the force acting in the longitudinal direction (x-axis, also the direction from subject to robot).

3.1. Load force tracking

To asses the difficulty of the given tasks, load force tracking accuracy ($Tacc_{F_{\mathrm{L}}}$) is introduced [23]:

$$Tacc_{F_{\mathrm{L}}} = 1 - \sqrt{\frac{\sum_{t=0\ \mathrm{s}}^{25\ \mathrm{s}} (|F_{\mathrm{virt}}| - |F_{\mathrm{L}}|)^2}{\sum_{t=0\ \mathrm{s}}^{25\ \mathrm{s}} |F_{\mathrm{virt}}|^2}}, \tag{4}$$

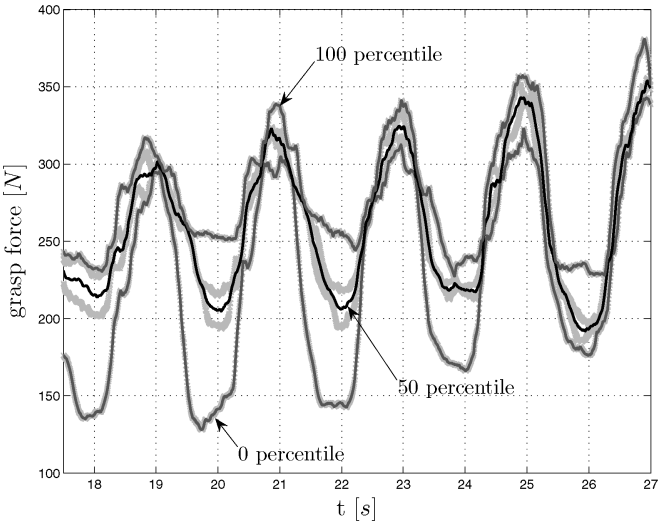

Figure 5. Fat light grey lines present four separate trials, dark grey lines represent 0 and 100 percentiles and black lines represent a 50 percentile. It can be clearly seen that the 0 percentile forms the lower bound and none of the samples of four trials is below this bound. Similarly, the 100 percentile forms the upper bound and none of the samples is above the upper bound.

where F_{virt} is the virtual load force and F_{L} is the force measured in the opposite direction to the virtual load force F_{virt}. Data for $Tacc_{F_{\text{L}}}$ in Tables 1 and 2 show that all subjects track F_{virt} with very high accuracy (average 99.5% for the ramp task and average 94.2% for the sinusoidal task when the amplitude is increasing, and average 99.4% for the ramp task and average 94.2% for the sinusoidal task when the amplitude is decreasing).

The correlation coefficient $CorrCoef_{\text{LG}}$ between the grasp force and load force F_{L} time series was calculated to estimate the coordination between the load and grasp force. This measure is considered as a sensitive parameter for precision of the coupling between the grasp and load force [16]. A very high correlation between the grasp and load forces (see Tables 1 and 2) is achieved for the ramp task where the average value of the correlation coefficient is 0.97 when the amplitude is increasing and 0.99 when the amplitude is decreasing, while the average value of the correlation coefficient 0.81 when the amplitude is increasing and 0.70 when the amplitude is decreasing for the sinusoidal task shows a degraded coordination of grasp and load force. The degradation of the coordination of the grasp and load force for the sinusoidal task is bigger when the amplitude is decreasing, otherwise there is no significant difference between experiments with increasing or decreasing amplitude.

From all four trials, the upper and lower time series bound of the grasp force was calculated (100 and 0 percentile in Fig. 5). A 50 percentile of four grasp force time series was subtracted from lower and upper bounds, and normalized with the 50 percentile. Equation (5) and Fig. 5 give a further explanation of the measure

Table 1.
Results when amplitude was increasing for load force tracking accuracy $Tacc_{F_L}$, correlation coefficient $CorrCoef_{LG}$ and intra-subject variability $bound_G$ (SD of four trials is given in parentheses)

Subject	$Tacc_{F_L}$ (%)		$CorrCoef_{LG}$		$bound_G$ (%)	
	Ramp	Sine	Ramp	Sine	Ramp	Sine
1	99.4 (0.2)	92.6 (1.3)	0.99 (0.01)	0.84 (0.03)	8.9	12.5
2	99.4 (0.1)	93.8 (0.2)	0.96 (0.01)	0.82 (0.03)	10.2	14.3
3	99.6 (0.2)	96.3 (0.6)	0.93 (0.06)	0.77 (0.04)	16.2	26.9
4	99.6 (0.1)	92.6 (1.3)	0.99 (0.01)	0.80 (0.07)	13.7	18.7
5	99.6 (0.1)	95.8 (1.1)	0.98 (0.01)	0.83 (0.08)	16.6	20.8
Average	99.5 (0.3)	94.2 (2.1)	0.97 (0.04)	0.81 (0.12)	13.1 (3.5)	18.7 (5.7)

Table 2.
Results when amplitude was decreasing for load force tracking accuracy $Tacc_{F_L}$, correlation coefficient $CorrCoef_{LG}$ and intra-subject variability $bound_G$ (SD of four trials is given in parentheses)

Subject	$Tacc_{F_L}$ (%)		$CorrCoef_{LG}$		$bound_G$ (%)	
	Ramp	Sine	Ramp	Sine	Ramp	Sine
1	99.6 (0.0)	92.1 (1.4)	0.99 (0.00)	0.83 (0.01)	17.6	10.3
2	99.4 (0.0)	95.0 (0.4)	0.99 (0.00)	0.67 (0.06)	9.2	14.6
3	99.1 (0.2)	92.3 (1.4)	0.99 (0.01)	0.70 (0.04)	10.8	17.9
4	99.5 (0.1)	95.8 (0.2)	0.98 (0.02)	0.64 (0.05)	18.3	12.2
5	99.6 (0.1)	95.7 (0.9)	0.99 (0.01)	0.65 (0.03)	14.1	19.2
Average	99.4 (0.1)	94.2 (1.5)	0.99 (0.01)	0.70 (0.07)	14.0 (4.0)	14.8 (3.8)

$bound_G$:

$$bound_G = \max\left(\frac{\sum_{t=0\ s}^{25\ s}|p^{100}(t) - p^{50}(t)|}{\sum_{t=0\ s}^{25\ s}|p^{50}(t)|}, \frac{\sum_{t=0\ s}^{25\ s}|p^{0}(t) - p^{50}(t)|}{\sum_{t=0\ s}^{25\ s}|p^{50}(t)|}\right). \quad (5)$$

The measure $bound_G$ gives information about the intra-subject variability. $bound_G$ shows an average 13.1% (amplitude increasing) and 14.0% (amplitude decreasing) for the ramp task and average 18.7% (amplitude increasing) and 14.8% (amplitude decreasing) intra-subject variability for the sinusoidal task (see Tables 1 and 2). The resulting bound given in the last two columns is the averaged maximum deviation of the grasp force of four trials. Additionally, low values of standard deviation for $Tacc_{F_L}$ and $CorrCoef_{LG}$ also show low intra-subject variability. Average values of all parameters (last row of Tables 1 and 2) also show low inter-subject variability.

3.2. Grasp force to load force ratio

Plots of grasp force *versus* load force show a distinctive shape for the ramp and sinusoidal tasks (see Figs 6 and 7 for experiments when the amplitude is increasing,

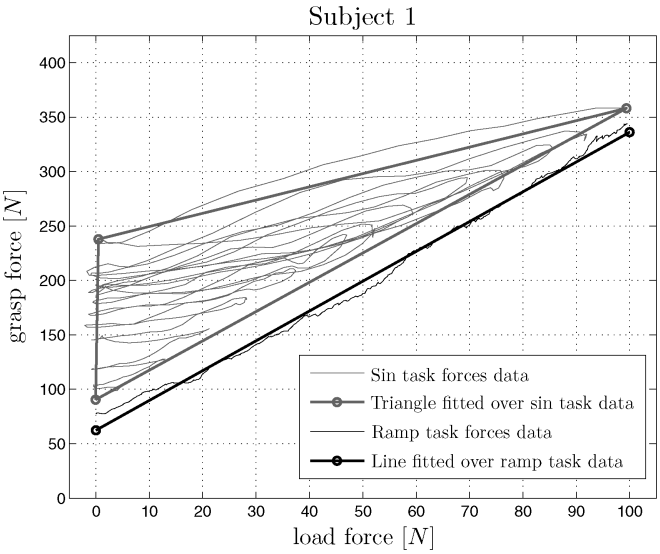

Figure 6. Grasp force *versus* load force plot for subject 1. A straight line is fitted over the ramp task data (dark line) and a triangle over the sinusoidal task (light gray). Time series are given in Fig. 4.

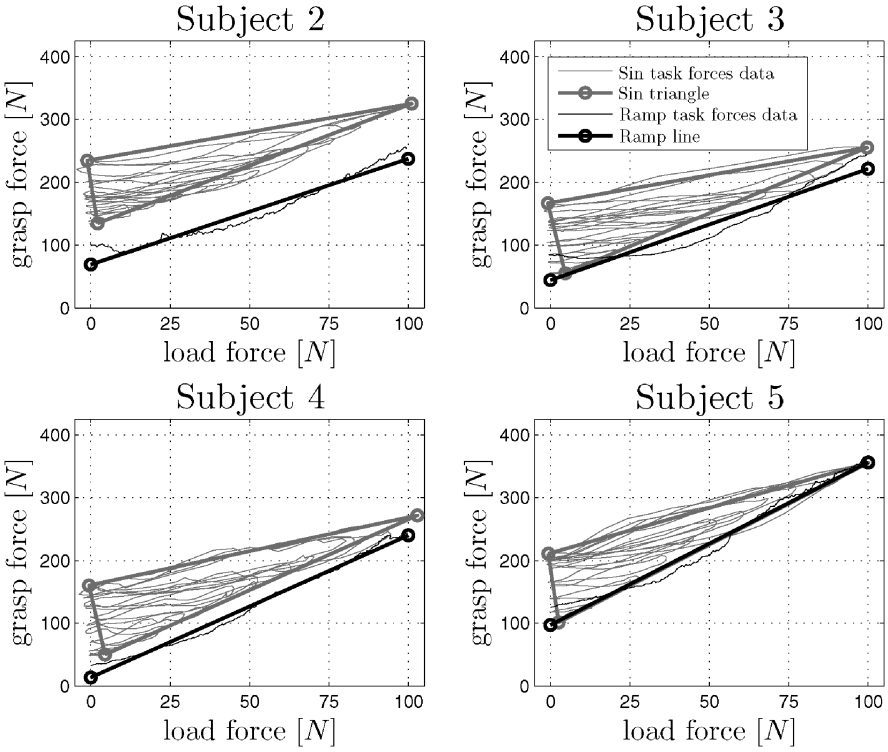

Figure 7. Grasp force *versus* load force plots for subjects 2–5 when the amplitude is increasing.

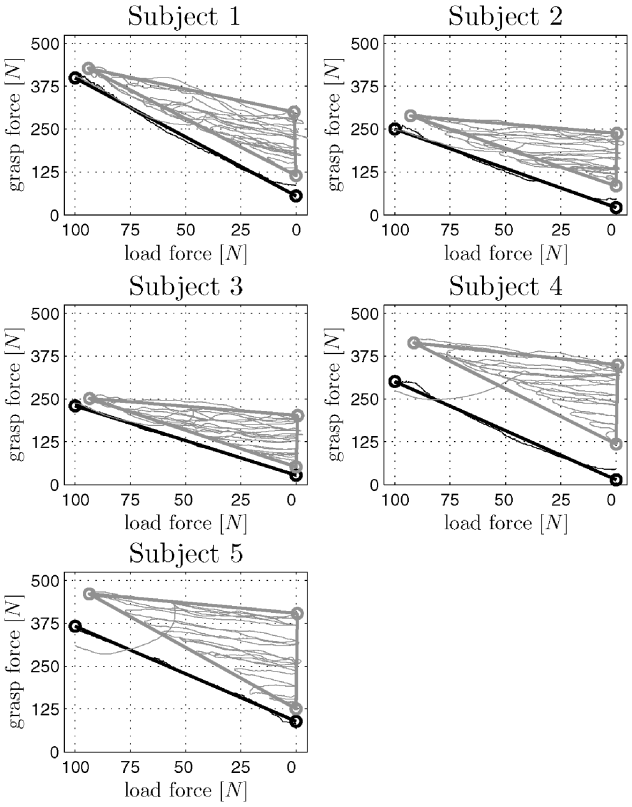

Figure 8. Grasp force *versus* load force plots for subjects 1–5 when the amplitude is decreasing.

and Fig. 8 for experiments when the amplitude is decreasing). The ramp task can be described with the linear function $F_{G,R} = k_R F_L + n_R$, while the sinusoidal task can be described with a characteristic triangle fitted over F_G/F_L data. The triangle fitted over F_G/F_L sinusoidal data is a triangle with the biggest area that fits in a convex hull enclosing the F_G/F_L sinusoidal data. The triangle can be described with a linear function $F_{G,S} = k_S F_L + n_S$ for a lower side of the triangle and square root of triangle area $\sqrt{p}$. $F_{G,R}$ stands for grasp force for the ramp task and $F_{G,S}$ for grasp force for the sinusoidal task.

The average square root of the area of the triangle $\sqrt{p}$ is 75 N (amplitude increasing, Table 3) and 95.9 N (amplitude decreasing, Table 4). The relative difference of k_s and k_r (measure $|k_s - k_r|/k_r$) shows that functions $F_{G,R}$ and $F_{G,S}$ are close to parallel. The normalized mean absolute difference of k_s and k_r is 7.1% with a standard deviation of 7.2% (amplitude increasing, Table 3) and 10.8% with a standard deviation of 11.1% (amplitude decreasing, Table 4).

Table 3.
Analysis of grasp force *versus* load force when amplitude is increasing

Subject	$\sqrt{p}$ (N)	$k_s \left(\frac{N}{N}\right)$	$k_r \left(\frac{N}{N}\right)$	$\frac{\lvert k_s - k_r \rvert}{k_r}$ (%)	n_s (N)	n_r (N)
1	78.3	2.54	2.50	1.6	100.7	72.7
2	72.6	1.81	1.52	19.0	137.0	72.8
3	72.2	1.86	1.97	5.6	50.8	40.9
4	76.1	2.08	2.27	8.1	48.5	13.3
5	76.0	2.55	2.59	1.4	94.2	97.3
Average	75.0 (2.5)	2.17 (0.36)	2.17 (0.43)	7.1 (7.2)	86.2 (37.2)	59.4 (32.7)

Table 4.
Analysis of grasp force *versus* load force when amplitude is decreasing

Subject	$\sqrt{p}$ (N)	$k_s \left(\frac{N}{N}\right)$	$k_r \left(\frac{N}{N}\right)$	$\frac{\lvert k_s - k_r \rvert}{k_r}$ (%)	n_s (N)	n_r (N)
1	92.6	3.33	3.44	3.3	114.1	55.0
2	84.8	2.21	2.30	3.7	83.9	21.4
3	84.1	2.13	2.03	5.0	52.0	27.2
4	103.4	3.24	2.87	12.6	118.4	13.5
5	114.6	3.59	2.77	29.6	125.9	89.5
Average	95.9 (13.0)	2.90 (0.68)	2.68 (0.55)	10.8 (11.1)	98.8 (30.7)	41.3 (31.1)

4. DISCUSSION

Coupling and coordination of the grasp and load force during quasi-static (ramp task) and dynamic (sinusoidal task) conditions is demonstrated in this paper. While for the ramp task more or less expected results are obtained, in cases where coordination of the grasp and load force is high (average correlation coefficients are 0.97 when the amplitude is increasing and 0.99 when the amplitude is decreasing; see Tables 1 and 2), the sinusoidal task shows degradation of grasp/load force coordination (correlation coefficient 0.81 with amplitude increasing and 0.70 with amplitude decreasing, see Tables 1 and 2) and a steady elevation of the grasp force.

Elevation of the grasp force was observed in children [13, 22], where elevation of the grasp force was ascribed to yet not fully developed sensory–motor mechanisms engaged in the control of dexterous manipulation in small children. Gilles and Wing [15] observed elevated grasp forces in elderly people and they discovered that elevation of the grasp force occurs due to lower coefficients of friction, caused by skin changes with age and not due to impairment of the sensory–motor mechanism. Rost *et al.* [16] studied grasp elevation in cerebellar patients, where elevation of the grasp force was caused by cerebellar impairment. The coordination of the grasp/load forces is automatically adjusted to the frictional conditions, providing a relatively small safety margin against slip [13]. In all experimental studies healthy adult subjects served as a control group.

The muscles for producing the force in the fingers are extrinsic and intrinsic muscles. Extrinsic muscles originate primarily in the forearm and provide strength, while intrinsic muscles originate primarily in the hand and provide precise coordination of the fingers. The main muscles for flexion of the fingers are the *flexor digitorum profundus* (FDP) and the *flexor digitorum superficialis* (FDS), which are extrinsic muscles. Both are the focal generators of flexion force at the distal and proximal interphalangeal joints (fingertips) [24]. FDP performs most of the unloaded finger flexion, while FDS provides additional strength, as in the case of the power grasp. Five primary muscles are involved in wrist and hand motion, while FDP and FDS are secondary muscles to rotate the wrist [25]. Muscles that cross more than one joint contribute simultaneously to the torques developed at all the spanned joints [26]. There is a noticeable mechanical coupling between wrist extension/flexion and finger flexion/extension know as tenodesis, which is often enhanced for the purpose of tenodesis grasp (grasp opening with wrist flexion and closing with wrist extension) in patients with tetraplegia [27]. Stimulation of the muscles for hand grasp and wrist extension must be coordinated because of an anatomical coupling between the joints introduced by the multiarticular extrinsic hand muscles [28, 29]. In addition, no mechanical coupling was found between elbow extension/flexion and movement of the wrist and fingers that should be compensated for, and elbow extension control was added solemnly to compensate for gravitational moments [30, 31]. Since there exists mechanical coupling between the wrist and fingers, and a high correlation coefficient $CorrCoef_{\mathrm{LG}}$ between the grasp force and load force F_{L} could be related to that phenomena, researchers agree that the nervous system is the one that maintains a precise balance between forces normal and tangential to the grasp surface through a sophisticated blend of feedforward and feedback sensory-motor control mechanisms [32–34].

The assumption is made that healthy adult subjects employ a close to optimal scheme for control of the grasp/load force for given frictional conditions. This assumption is based on the high accuracy of load force tracking (average value of $Tacc_{F_{\mathrm{L}}}$ 99.5% with amplitude increasing and 99.4% with amplitude decreasing), high value of the correlation coefficient between grasp and load force (average values of 0.97 and 0.99 for $CorrCoef_{\mathrm{LG}}$) and low intra-subject variability (average values of 13.1 and 14.0% for $bound_{\mathrm{G}}$) for the quasi-static (ramp) task.

The relation between load force F_{L} and grasp force F_{G} in quasi-static conditions is described by the following expression:

$$F_{\mathrm{G}}(t) = k_{\mathrm{slip}} F_{\mathrm{L}}(t) + F_{\mathrm{Gi}}, \tag{6}$$

where F_{Gi} is the grasp force in the resting position at $F_{\mathrm{L}} = 0$ N and k_{slip} is slip the coefficient as the inverse of the friction coefficient. Data for the ramp task (quasi-static) show that subjects grasp with some initial grasp force even when there are no longitudinal external load forces. This grasp force can result from a comfortable initial grasp force.

Under dynamic conditions, an additional margin of safety is required in order to maintain the grasp [35]. Experimental data show that elevation of grasp force occurs in the dynamic task (see Fig. 4e and g). In plots of F_G *versus* F_L this elevation of grasp force can be seen as formation of a triangular shape when the amplitude of the load force is increasing (see Figs 6–8). Figures 6–8 represent experiments with the ramp and sinusoidal force at 0.5 Hz. To show the course of gradual formation of the triangle, further experiments with a sinusoidal load force having frequencies of 0.1, 0.2, 0.5 and 1.0 Hz were performed with one person (subject 3). For each frequency the experiment was repeated 4 times. Table 5 shows the results of the experiments, while Fig. 9 gives a graphical interpretation of the obtained results. A triangle forms already at a frequency of 0.1 Hz; with a frequency increase, the area of the triangle gets bigger, while k_s remains relatively unchanged. This is represented by gray arrows in Fig. 9; the direction of arrows corresponds to the rise

Table 5.
Results of experiments with four different frequencies of the sinusoidal experiment

Frequency (Hz)	$\sqrt{p}$ (N)	$k_s \left(\frac{N}{N}\right)$	n_s (N)	$\frac{\lvert k_s - k_r \rvert}{k_r}$ (%)	$bound_G$ (%)
0.1	14.7	2.13	43.6	5.1	12.5
0.2	64.9	2.07	51.1	2.0	17.9
0.5	84.1	2.13	52.0	5.0	17.9
1.0	108.1	2.28	91.6	12.4	12.7

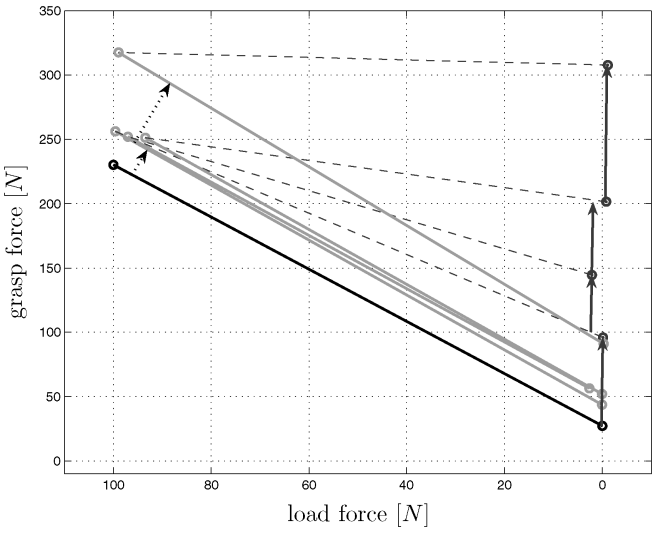

Figure 9. Formation of the triangular shape of the grasp to load force plots with increasing frequency of the sinusoidal load force. Grey arrows show the gradual increase of the triangle area with increasing frequency, while the slope (k_s) of the lower side of the triangle stays unchanged and in parallel with the slope (k_r) of the ramp experiment.

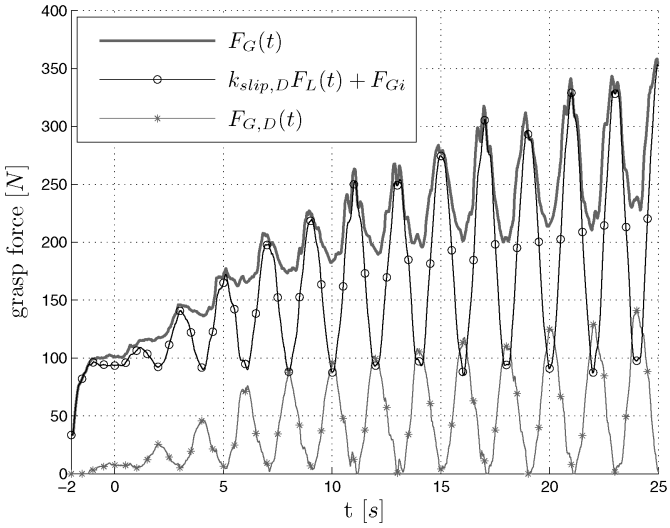

Figure 10. Decomposition of the grasp force for the sinusoidal task.

of frequency of sinusoidal load force. Black dotted arrows show the rise of the lower side of triangle towards the higher grasp forces with the rise of the frequency of the sinusoidal load force. After taking into consideration the comfort of the subjects and the triangle with the biggest area for good representation of the phenomena, the frequency of 0.5 Hz was chosen as the sinusoidal load force for experiments conducted with other subjects.

For dynamic conditions, scheme (6) has to be updated with the dynamic term of the grasp force:

$$F_{\mathrm{G}}(t) = k_{\mathrm{slip,D}} F_{\mathrm{L}}(t) + F_{\mathrm{Gi}} + F_{\mathrm{G,D}}(t), \tag{7}$$

where $F_{\mathrm{G,D}}$ is a task-dependant dynamic term of the grasp force F_{G}. Note that no assumption is made that $k_{\mathrm{slip}} = k_{\mathrm{slip,D}}$, yet measure $|k_{\mathrm{s}} - k_{\mathrm{r}}|/k_{\mathrm{r}}$ (see Tables 3 and 4) shows that k_{slip} in ramp and sinusoidal tasks does not differ significantly. Data show that the difference between k_{slip} and $k_{\mathrm{slip,D}}$ is 7% with a standard deviation of 7% (amplitude increasing) and 11% with a standard deviation of 11% (amplitude decreasing). This implies that perception of slippage does not change.

Figure 10 shows the decomposition of the grasp force $F_{\mathrm{G}}(t)$ for the sinusoidal task.

Decomposition shows that $F_{\mathrm{G,D}}(t)$ increases when $k_{\mathrm{slip,D}} F_{\mathrm{L}}(t)$ decreases every period of the sinusoidal time series. $F_{\mathrm{G,D}}(t)$ represents the additional grasp force (last term in (7)) for compensating for the potential loss of stability when $k_{\mathrm{slip,D}} F_{\mathrm{L}}(t) + F_{\mathrm{Gi}}$ drops below a certain margin of F_{G} which is needed for a stable grasp.

Next, the possible link between $F_{\mathrm{G,D}}$ with kinematic variables acceleration, velocity and position is investigated. Table 6 shows the correlation coefficient between $F_{\mathrm{G,D}}(t)$ and acceleration related to the given trial. Correlation is high and

Table 6.
Analysis of correlation coefficient between $F_{G,D}$ and acceleration, velocity and position (SD of four trials is given in parentheses)

Subject	$CorrCoef_{accE,GE}$	$CorrCoef_{velE,GE}$	$CorrCoef_{posE,GE}$
1	0.87 (0.04)	0.84 (0.04)	0.76 (0.12)
2	0.78 (0.08)	0.73 (0.09)	0.63 (0.04)
3	0.87 (0.05)	0.85 (0.07)	0.87 (0.03)
4	0.91 (0.06)	0.88 (0.07)	0.88 (0.07)
5	0.77 (0.11)	0.76 (0.15)	0.62 (0.18)
Average	0.84 (0.15)	0.81 (0.19)	0.75 (0.20)

supports the assertion that an additional margin of safety is required in order to maintain the stability of grasp under dynamic conditions. The correlation between $F_{G,D}(t)$ and the velocity and position is also given. Data shows slightly lower correlation for velocity and position with $F_{G,D}(t)$.

5. CONCLUSIONS

In this paper, a new instrumentation approach and new experimental procedure for evaluation of grasp is introduced. A combination of a haptic interface with force/torque transducers for measuring grasp force shows a great potential for studying grasp in humans. The general framework allows use of a diverse external load force time series, virtual environments and human–robot interfaces (different handles for different types of grasps).

This paper also presents results of grasp and load forces in positioning tasks under external force disturbances (ramp and sinusoidal time series). A linear relation between load force F_L and grasp force F_G was experimentally confirmed for the ramp task. Results show elevation of the grasp force in the dynamic (sinusoidal) task and a distinctive triangular shape was observed for grasp *versus* load force representation. Decomposition into linear, initial and dynamic parts of the grasp force is proposed. Elevation of the grasp force is needed in dynamic conditions to assure a stable grasp.

A potential of this study can be seen in human–robot cooperation. This study presents results for human grasping, when a robot is a source of external force disturbances. However, the situation can be reversed. A human can be a source of external disturbances and a robot cooperates with a human, holding the object on which the human exerts external forces [36, 37].

Acknowledgements

The authors wish to acknowledge financial support from the Republic of Slovenia Ministry of Higher Education, Science and Technology.

REFERENCES

1. J. R. Napier, The prehensile movements of the human hand, *J. Bone Joint Surg. Br.* **38B**, 902–913 (1956).
2. M. R. Cutkosky, On grasp choice, grasp models, and the design of hands for manufacturing tasks, *IEEE Trans. Robotics Automat.* **5**, 269–279 (1989).
3. S. Kang and K. Ikeuchi, Toward automatic robot instruction from perception: recognizing a grasp from observation, *IEEE Trans. Robotics Automat.* **9**, 432–443 (1993).
4. G. A. Bekey, H. Liu, R. Tomovic and W. J. Karplus, Knowledge-based control of grasping in robot hands using heuristics from human motor skills, *IEEE Trans. Robotics Automat.* **9**, 709–722 (1993).
5. S. Kang and K. Ikeuchi, Toward automatic robot instruction from perception — temporal segmentation of tasks from human hand motion, *IEEE Trans. Robotics Automat.* **11**, 670–681 (1995).
6. T. Iberall, Human prehension and dexterous robot hands, *Int. J. Robotics Res.* **16**, 285–299 (1997).
7. J. Ueda, R. Negi and T. Yoshikawa, Acquisition of a page turning skill for a multifingered hand using reinforcement learning, *Advanced Robotics* **18**, 101–114 (2004).
8. M. Hershkowitz, U. Tasch and M. Teboulle, Toward a formulation of the human grasping quality sense, *J. Robot Syst.* **12**, 249–256 (1995).
9. K. B. Shimoga, Robot Grasp Synthesis Algorithms: a survey, *Int. J. Robotics Res.* **15**, 230–266 (1996).
10. V. D. Nguyen, Constructing force-closure grasp, *Int. J. Robotics Res.* **7**, 3–16 (1988).
11. M. Lim, S. Oh, J. Son, B. You and K. Kim, A human-like real-time grasp synthesis method for humanoid robot hands, *Robotics Autonomous Syst.* **30**, 261–271 (2000).
12. S. Jaric, E. M. Russell, J. J. Collins and R. Marwaha, Coordination of hand grip and load forces in uni- and bidirectional static force production tasks, *Neurosci. Lett.* **381**, 51–56 (2005).
13. H. Forssberg, A. C. Eliasson, H. Kinoshita, G. Westling and R. S. Johansson, Development of human precision grip. IV. Tactile adaptation of isometric finger forces to the frictional condition, *Exp. Brain Res.* **104**, 323–330 (1995).
14. A. C. Eliasson, H. Forssberg, K. Ikuta, I. Apel, G. Westling and R. S. Johansson, Development of human precision grip. V. Anticipatory and triggered grip actions during sudden loading, *Exp. Brain Res.* **106**, 425–433 (1995).
15. M. A. Gilles and A. M. Wing, Age-related changes in grip force and dynamics of hand movement, *J. Motor Behav.* **35**, 79–85 (2003).
16. K. Rost, D. A. Nowak, D. Timmann and J. Hermsdörfer, Preserved and impaired aspects of predictive grip force control in cerebellar patients, *Clin. Neurophysiol.* **116**, 1405–1414 (2005).
17. R. J. Adams and B. Hannaford, Stable haptic interaction with virtual environments, *IEEE Trans. Robotics Automat.* **15**, 465–474 (1999).
18. M. Ponikvar, M. Munih, J. Hoogen, G. Schmidt and R. Riener, Haptic environment for analysis of smooth arm movements, in: *Proc. Int. Conf. on Advanced Robotics*, Coimbra, pp. 173–178 (2003).
19. JR3, *Installation Manual for Force–Torque Sensors with Internal Electronics*. JR3, Woodland, CA (2001).
20. R. W. McGorry, A system for the measurement of grip forces and applied moments during hand tool use, *Appl. Ergon.* **32**, 271–279 (2001).
21. E. K. J. Chadwick and A. C. Nicol, A novel force transducer for the measurement of grip force, *J. Biomech.* **34**, 125–128 (2001).
22. C. S. Edgren, R. G. Radwin and C. B. Irwin, Grip force vectors for varying handle diameters and hand sizes, *Human Factors* **46**, 244–351 (2004).

23. R. D. Jones, Measurement of sensory-motor control performance capacities: tracking tasks, in: *The Biomedical Engineering Handbook*, J. D. Bronzino (Ed.), pp. 2197–2218. CRC Press, Boca Raton, FL (2000).
24. M. Shinohara, M. L. Latash and V. M. Zatsiorsky, Age effects on force produced by intrinsic and extrinsic hand muscles and finger interaction during MVC tasks, *J. Appl. Physiol.* **95**, 1361–1369 (2003).
25. A. Freivalds, Models of the upper limbs, in: *Biomechanics of the Upper Limbs: Mechanics, Modeling, and Musculoskeletal Injuries*, pp. 195–222. CRC Press, Boca Raton, FL (2004).
26. B. A. Garner and M. G. Pandy, Estimation of musculotendon properties in the human upper limb, *Ann. Biomed. Eng.* **31**, 207–220 (2003).
27. M. B. Popovic, Control of neural prostheses for grasping and reaching, *Med. Eng. Phys.* **25**, 4150 (2003).
28. M. M. Adamczyk and P. E. Crago, Simulated feedforward neural network coordination of hand grasp and wrist angle in a neuroprosthesis, *IEEE Trans. Rehabil. Eng.* **8**, 297–304 (2000).
29. T. R. D. Scott, L. Atmore, J. M. Heasman, R. Y. Flynn, V. A. Vare and C. Gschwind, Synergistic control of stimulated pronosupination with the stimulated grasp of persons with tetraplegia, *IEEE Trans. Rehabil. Eng.* **9**, 258–264 (2001).
30. J. H. Grill and P. H. Peckham, Functional neuromuscular stimulation for combined control of elbow extension and hand grasp in C5 and C6 quadriplegics, *IEEE Trans. Rehabil. Eng.* **6**, 190–199 (1998).
31. P. E. Crago, W. D. Memberg, M. K. Usey, M. W. Keith, R. F. Kirsch, G. J. Chapman, M. A. Katorgi and E. J. Perreault, An elbow extension neuroprosthesis for individuals with tetraplegia, *IEEE Trans. Rehabil. Eng.* **6**, 1–6 (1998).
32. R. S. Johansson, Sensory control of dextrous manipulation in humans, in: *Hand and Brain: The Neurophysiology and Psychology of Hand Movements*, A. M. Wing, P. Haggard and J. R. Flanagan (Eds), pp. 381–414. Academic Press, San Diego, CA (1996).
33. V. M. Zatsiorsky, Z. M. Li and M. L. Latash, Enslaving effects in multi-finger force production, *Exp. Brain Res.* **131**, 187–195 (2000).
34. M. L. Latash, S. Li, F. Danion and V. M. Zatsiorsky, Central mechanisms of finger interaction during one- and two-hand force production at distal and proximal phalanges, *Brain Res.* **924**, 198–208 (2002).
35. R. G. Bonitz and T. C. Hsia, Robust dual-arm manipulation of rigid objects via palm grasping, in: *Proc. IEEE Trans. on Robotics and Automation*, Minneapolis, MN, pp. 3047–3054 (1996).
36. J. Kim, J. Park, Y. K. Hwang and M. Lee, Advanced grasp planning for handover operation between human and robot: three handover methods in esteem etiquettes using dual arms and hands of home-service robot, in: *Proc. Int. Conf. on Autonomous Robots and Agents December*, Palmerston North, pp. 13–15 (2004).
37. H. Iwata and S. Sugano, Human robot interference adapting control coordinating human following and task execution, in: *Proc. Int. Conf. on Intelligent Robots and Systems*, Sendai, pp. 2879–2885 (2004).

ABOUT THE AUTHORS

Janez Podobnik received the BSc degree in Electrical Engineering in 2004 from the Faculty of Electrical Engineering, University of Ljubljana, Slovenia. Since 2004, he has been working as a PhD Student as part of a research team at the Laboratory of Robotics and Biomedical Engineering, Faculty of Electrical Engineering, University of Ljubljana. His main research activity is in the field of rehabilitation robotics and haptic interfaces.

Marko Munih received the BSc, MSc and DSc degrees in Electrical Engineering from the University of Ljubljana, Slovenia, in 1986, 1989 and 1993, respectively. His research interests were focused in functional electrical stimulation of paraplegic lower extremities with surface electrode systems, including measurements, control, biomechanics and electrical circuits. From 1989, he was Teaching Assistant and from 1997 Assistant Professor at the Faculty of Electrical Engineering, Ljubljana. From 1995 to 1996, he was a Research Assistant with the Implanted Devices Group, Department of Medical Physics and Bioengineering, University College London and Royal National Orthopaedic Hospital Trust, Stanmore, UK. In the last period his interest focused on robot contact with the environment and use of haptic interfaces in the field of rehabilitation engineering (projects GENTLE/S, I-Match, Alladin). He was the recipient of the Zois award in 2002, given for outstanding scientific contributions by the Slovene Ministry of Science, Education and Sport. Currently, he is Professor and Head of the Laboratory of Robotics and Biomedical Engineering, Faculty of Electrical Engineering, Ljubljana. He is a member of the IEEE, IFMBE, IFESS and IFAC.